Motion Control of Piezoelectric Positioning Stages: Modeling, Controller Design, and Experimental Evaluation

Guo-Ying Gu, *Student Member, IEEE*, Li-Min Zhu, *Member, IEEE*, Chun-Yi Su, *Senior Member, IEEE*, and Han Ding, *Senior Member, IEEE*

***Abstract*—In this paper, a general skeleton on modeling, controller design, and applications of the piezoelectric positioning stages is presented. Toward this framework, a general model is first proposed to characterize dynamic behaviors of the stage, including frequency response of the stage, voltage–charge hysteresis and nonlinear electric behavior. To illustrate the validity of the proposed general model, a dynamic backlash-like model is adopted as one of hysteresis models to describe the hysteresis effect, which is confirmed by experimental tests. Thus, the developed model provides a general frame for controller design. As an illustration to this aspect, a robust adaptive controller is developed based on a reduced dynamic model under both unknown hysteresis nonlinearities and parameter uncertainties. The proposed control law ensures the boundedness of the closed-loop signals and desired tracking precision. Finally, experimental tests with different motion trajectories are conducted to verify the proposed general model and the robust control law. Experimental results demonstrate the excellent tracking performance, which validates the feasibility and effectiveness of the proposed approach.**

***Index Terms*—Electromechanical model, hysteresis, motion control, piezoelectric positioning stage, robust control.**

I. Introduction

ALONG with the rapid development of nanoscience and nanotechnology, piezoelectric positioning stages are becoming more and more popular for nanometer or subnanometer displacement resolution in many industrial applications [1]–[5], including atomic force microscopes, scanning tunneling microscopes, micromanipulation, etc. A piezoelectric positioning stage system typically consists of four components: a flexure-hinge-based mechanism, a piezoelectric ceramic actuator (PCA), a piezoelectric drive circuit, and a displacement sensor. Such a mechatronic system has attracted significant attention in the literature on its modeling, controller design, and applications due to the complex hysteresis nonlinearity exhibited in the PCA [6]–[11]. Generally speaking, the modeling and controller design are closely related and the models of the piezoelectric positioning stages should account for dynamic effects due to frequency response of the actuator, voltage–charge hysteresis, and nonlinear electric behavior. However, in previous discussions the attention was mainly paid to different aspects with different assumptions. For example, in [8] and [10], the stages were described by a linear system preceded by a hysteresis nonlinearity and the main focus is on hysteresis compensations. In [8], an inverse hysteresis compensation was adopted where the system was assumed to be a first-order linear system. In [10], a robust control approach was developed to compensate for the hysteresis effects where the system was assumed to be a second-order system. On the other hand, in [6], [7], [9], and [11], the hysteresis nonlinearities were treated as disturbances and the stages were described by linear systems with different assumptions on system orders. Then, different control approaches were developed.

It is obvious from the above discussions, a general skeleton on modeling, controller design, and applications of the piezoelectric positioning stages is still missing. Based on the above accumulated results, it is now ready to develop a united description of the stage, reflecting dynamic effects due to frequency response of the actuator, voltage-charge hysteresis, and nonlinear electric behavior, so that any stage model assumed in the literature can be deduced from it, depending on the applications. With this general description of the stages, different control strategies for various applications can thus be developed.

Toward this general framework, in this paper we present a comprehensive study on modeling, controller design, and experimental evaluation for the piezoelectric positioning stages. A general model is first proposed to represent the dynamic behaviors of the stage including both electrical and mechanical components. To illustrate the validity of the general model, a dynamic backlash-like hysteresis model is adopted as one of hysteresis models to describe the hysteresis effect in the stage. Experimental tests confirm such a description. To further demonstrate the benefits of this general model, a reduced dynamic model is used to develop a robust adaptive controller (RAC) under both unknown hysteresis nonlinearities and

Manuscript received September 6, 2011; revised February 19, 2012 and April 25, 2012; accepted May 28, 2012. Date of publication June 22, 2012; date of current version July 11, 2013. Recommended by Technical Editor G. Liu. This work was supported in part by the National Natural Science Foundation of China under Grant 91023047, in part by the Science and Technology Commission of Shanghai Municipality under Grant 11520701500, and in part by the Shu Guang Project supported by Shanghai Municipal Education Commission under Grant 10SG17.

G.-Y. Gu, L.-M. Zhu, and H. Ding are with the State Key Laboratory of Mechanical System and Vibration, School of Mechanical Engineering, Shanghai Jiao Tong University, Shanghai 200240, China (e-mail: guguoying@sjtu.edu.cn; zhulm@sjtu.edu.cn; hding@sjtu.edu.cn).

C.-Y. Su is with the College of Automation Science and Engineering, South China University of Technology, Guangzhou 510641, China, on leave from Concordia University, Montreal, QC H3G 1M8, Canada (e-mail: cysu@alcor.concordia.ca).

Color versions of one or more of the figures in this paper are available online at http://ieeexplore.ieee.org.

Digital Object Identifier 10.1109/TMECH.2012.2203315

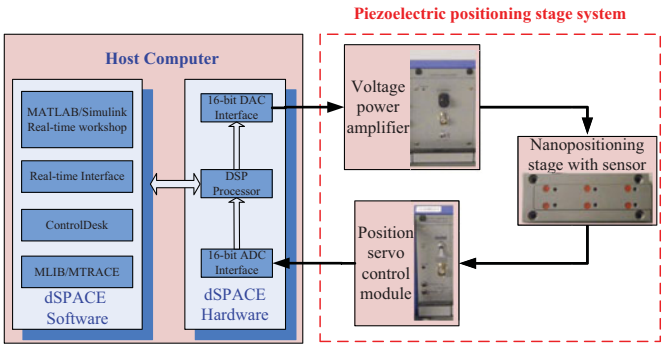

Fig. 1. Architecture of a piezoelectric positioning system.

parameter uncertainties. The proposed control law ensures the boundedness of the closed-loop signals and desired tracking precision. Finally, experimental tests with different motion trajectories are conducted to verify the effectiveness of the proposed general model and the corresponding robust controller design.

The remainder of this paper is organized as follows. Section II starts with description of the piezoelectric positioning stage. In Section III, a general model is proposed, and a RAC is then implemented in Section IV. In Section V, the experimental tests are conducted, and Section VI concludes this paper.

II. Description of Piezoelectric Positioning Stages

The architecture of a piezoelectric positioning stage as shown in Fig. 1 normally consists of a compact 1-D flexure-hinge-based stage with integrated capacitive gap sensors, a position servo-control module (PSCM), and a voltage power amplifier. Therein, 1) the flexure-hinge-based mechanism is utilized to provide motion based on elastic deformations of a solid part made from a stiff metal because of the advantages of its no sliding parts, thereby avoiding undesired nonlinear effects such as backlash and friction [12], [13]; 2) a PCA is applied to realize the actuation function by generating force on the mechanisms due to the excellent advantages of the large output force, high bandwidth and fast response time [14]; 3) a piezoelectric driver amplifier (PDA) is used to supply power for the PCA by either voltage control or charge control; 4) a displacement sensor with high resolution is utilized to measure the real-time motion displacement of the stage. Generally, capacitive sensors are adopted as a displacement sensor to achieve nanometer or subnanometer resolution due to its wide bandwidth and large dynamic rage [1].

As an example, a piezoelectric positioning stage (PZT mode P-753.31C produced by Physik Instrumente GmbH & Co.) is detailed as follows. PZT mode P-753.31C is driven by applied control input voltage in the range of -2 to 10 V and has nominal 38-μm expansion. The PDA is a voltage power amplifier with a fixed gain of 10 to amplify the control input for driving the PCA. The unloaded resonance frequency of the mechanical response is 2.9 kHz. The capacitive gap sensor is integrated in the mechanical structure to measure the displacement of the stage. The PSCM is then used to transfer the displacement to analogue voltage in the range of 0–10 V. The specifications of the piezoelectric positioning stage P-753.31C are listed in Table I.

TABLE I
Properties of the Piezoelectric Positioning Stage

Items	Piezoelectric positioning stage	Units
Driven voltage	-2 to 10	V
Expansion displacement	0 to 38	μm
Electrical capacitance	4.6	μF
Stiffness in motion direction	16	N/μm
Unloaded resonant frequency	2.9	kHz
Stage mass	0.25	kg
PSCM output	0 to 10	V

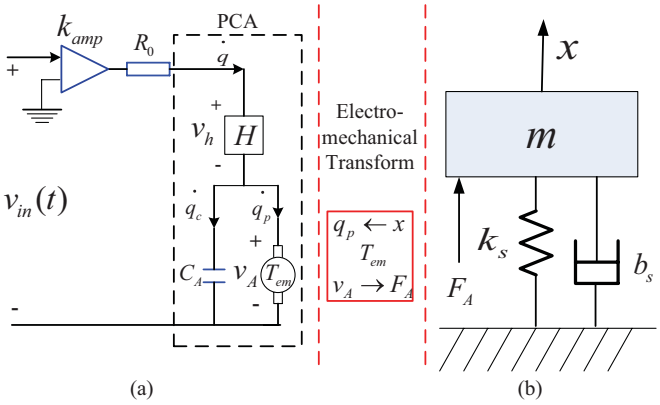

Fig. 2. General model of the piezoelectric positioning stage: (a) electrical aspect and (b) mechanical aspect.

III. Comprehensive Modeling Approach of Piezoelectric Positioning Stages

Following the accumulated research results developed for PCA in [15], [16], and [17], a general schematic model of a piezoelectric positioning stage can be represented by Fig. 2. In the following development, we shall use this structure as a base to completely represent the characteristics of the piezoelectric positioning stage, assembling to the traditional dc motor, which will be described from both electrical and mechanical aspects.

A. Electrical Modeling

From the electrical aspect, the piezoelectric positioning stage system can be modeled as an equivalent circuit as shown in Fig. 2(a), which is composed of a circuit of the PDA and a circuit of the PCA. From Fig. 2(a), the PDA is modeled as a fixed gain $k_{\rm amp}$ plus an equivalent internal resistance R_0 of the driving circuit, v_h is the generated voltage due to the hysteresis effect, $H(q)$, $T_{\rm em}$ represents the piezo effect, which is an electromechanical transducer with transformer ratio, and C_A represents the sum of the capacitances of the total piezoelectric ceramics, which is electrically in parallel with the transformer. The total charge in the PCA is q, and the resulting current flowing through the circuit is $\dot{q}$. The charge stored in the linear capacitance C_A is represented as q_c. The charge q_p is the transduced charge from the mechanical side due to the piezoelectric effect, the voltage v_A is the transduced voltage. The detailed descriptions of the notations related to piezoelectric actuators may refer to [15]

and [16]. Therefore, the complete electrical equations can be expressed as follows:

$$R_0\dot{q}(t) + v_h(t) + v_A(t) = k_{\rm amp}v_{\rm in}(t) \quad (1)$$

$$v_h(t) = H(q) \quad (2)$$

$$q(t) = q_c(t) + q_p(t) \quad (3)$$

$$v_A(t) = q_c(t)/C_A \quad (4)$$

$$q_p(t) = T_{\rm em}x(t) \quad (5)$$

where $v_{\rm in}$ is the control input for the PDA, x is the output displacement of the mechanical part, and $k_{\rm amp}$ is the fixed gain of the voltage power amplifier.

By substituting (2)–(5) into (1), the complete electrical equations can be further simplified as

$$R_0C_A\dot{q}(t) + q(t) - T_{\rm em}x(t) = C_Ak_{\rm amp}\left[v_{\rm in}(t) - \frac{H(q)}{k_{\rm amp}}\right]. \quad (6)$$

Remark: It is important to note it is R_0 that makes a difference in the electric part between the piezoelectric positioning stage and piezoelectric actuators in [15] and [16]. Although the set of linear constitutive equations presented in [15] and [16] are fine for many applications, a more realistic model requires the inclusion of R_0. Due to the existence of R_0 in the piezoelectric positioning stage, the electrical part can be expressed as a differential equation of the charge q. When $R_0 = 0$, it is reduced to the set of linear constitutive equations as discussed in [15] and [16], which cannot lead to (6). The role of (6) will be further explained in the following development.

B. Electromechanical Modeling

In mechanical aspect, the following dynamic electromechanical equations can be obtained according to the piezoelectric effect and Newton's laws of motion

$$F_A = T_{\rm em}v_A(t) \quad (7)$$

$$m\ddot{x}(t) + b_s\dot{x}(t) + k_sx(t) = F_A \quad (8)$$

where F_A is the transduced force from the electrical side; x is the output displacement of the mechanical part; m, b_s, and k_s are the mass, damping coefficient, and stiffness of the moving mechanism, respectively.

To present $v_A(t)$ in (7) in terms of $q(t)$, it is obvious from (3) to (5) that

$$v_A(t) = \frac{1}{C_A}q(t) - \frac{T_{\rm em}}{C_A}x(t). \quad (9)$$

The dynamic electromechanical (8) can then be rewritten as

$$m\ddot{x}(t) + b_s\dot{x}(t) + \overline{k_s}x(t) = \frac{T_{\rm em}}{C_A}q(t) \quad (10)$$

where $\overline{k_s} = k_s + \frac{T_{\rm em}^2}{C_A}$.

C. A General Dynamic Model

Combining the electrical model (6) and the electromechanical model (10), a general dynamic model of the piezoelectric positioning stage is represented by the following set of equations:

$$R_0C_A\dot{q}(t) + q(t) - T_{\rm em}x(t) = C_Ak_{\rm amp}[v_{\rm in}(t) - \frac{H(q)}{k_{\rm amp}}] \quad (11)$$

$$m\ddot{x}(t) + b_s\dot{x}(t) + \overline{k_s}x(t) = \frac{T_{\rm em}}{C_A}q(t). \quad (12)$$

These two equations represent an analytical model of the piezoelectric positioning stage, which surprisingly assembles to the model of the traditional permanent magnet dc motor.

Remarks:

1) A complete comprehensive model of the piezoelectric positioning stage system proposed in (11) and (12) accounts for both the dynamics of the piezoelectric positioning stage and the hysteresis inherent to the PCA. Surprisingly, until now there is no such a complete description available in the literature though a lot of papers have addressed this issue [7]–[11], [18], [19]. Possible reason is that the most of available results focused on a piezoelectric actuator itself, not on the stage, i.e., [15], [16], [20], [21], where the dynamic models consisting of a second-order linear plant with hysteresis nonlinearities, focused on the PCA and ignored R_0. The proposed model can be reduced to this case if the electric circuit of the PDA is neglected, that is $R_0 = 0$ in (6). On the other hand, Gao *et al*. [17] proposed a linear modeling approach including both PDA and PCA. However, the hysteresis effect of the PCA is ignored. The proposed model can also be reduced to this case without considering the hysteresis effect $H(q)$ in (11).
2) It is well known that dynamic model of a permanent magnet dc motor can be described as:

$$L\frac{i(t)}{dt} + Ri(t) + K_{\rm emf}\frac{\theta(t)}{dt} = v_{\rm in}(t) \quad (13)$$

$$J\ddot{\theta}(t) + B\dot{\theta}(t) = K_ti(t) \quad (14)$$

where i is the armature current, θ is the angular position, L, R, $K_{\rm emf}$, and K_t are motor's inductance, resistance, back-emf constant, and torque constant, respectively, J is the inertia of the rotor and the equivalent mechanical load, and B is the damping coefficient. From (11) to (12), it is amused that the dynamic model of the piezoelectric positioning stage is so similar to the traditional dc motor, except the hysteresis nonlinearity $H(q)$. Therefore, the challenge for control of the piezoelectric positioning stage system mainly lies on existence of the nonsmooth hysteresis nonlinearity $H(q)$, which usually degrades the system performance in such manners as giving rise to undesirable inaccuracies or oscillations, even leading to instability [22] in the closed-loop manner.
3) It is worth of mentioning that the charge control of PCA instead of the voltage control can eliminate the effect of hysteresis from (10), which is also demonstrated in [23] and [24]. This is exactly similar to directly control the armature current of a permanent magnet dc motor. However, as similar to the dc motor, the charge control has not been widely adopted due to the complicated implementation

of the power driver and the cost of such techniques [1]. Therefore, this paper discusses the related modeling and control problems when the voltage control approach is used.

D. Model Validation

To verify the proposed general dynamic model, a piezoelectric positioning stage (PZT mode P-753.31C produced by Physik Instrumente GmbH and Company) is used as a test bed which is described in Section II.

1) Gain of the PSCM: Before model validation, the gain $K_{\rm PSCM}$ of the PSCM used to transfer the displacement to analog voltage in the range of 0–10 V needs to be fixed, which is calculated as

$$K_{\rm PSCM} = 10/(x_{10} - x_0) \ \ ({\rm V}/\mu{\rm m}) \tag{15}$$

where x_{10} is the real-stage position when the sensor monitor output is 10 V, and x_0 is the real-stage position when the sensor monitor output reaches to 0 V. For this stage, $x_{10} = 38$ μm and $x_0 = 0$ μm, thus one can get $K_{\rm PSCM} = 10/38$ V/μm.

2) Identification of the Linear Dynamic Plant: Until now, there is no general approach to identify the parameters of the analytical model (11) and (12) due to the existence of the hysteresis nonlinearity. As a comprise, the commonly adopted approach in the literature is to express the analytical model into a linear system preceded by a hysteresis term. Then, the linear parameters and the hysteresis model will be identified separately [18], [25], [26]. In the following development, we will follow this line.

Since the PDA operates in the voltage control mode to supply charge for the PCA to generate the piezoelectric expansion, the induced charge $q(t)$ in the circuit should be represented as a function of control input $v_{\rm in}(t)$, that is, $q(t) = f(v_{\rm in}(t))$. Without loss of generality, the term $v_{\rm in}(t) - \frac{H(f(v_{\rm in})}{k_{\rm amp}}$ can be defined as a new hysteresis nonlinearity $P(v_{\rm in}(t))$

$$w(t) = P(v_{\rm in}(t)) \tag{16}$$

where $P(v_{\rm in}(t)) = v_{\rm in}(t) - \frac{H(f(v_{\rm in})}{k_{\rm amp}}$. In this case, the signal from $P(v_{\rm in}(t))$ to the output of the displacement x in (11) and (12) can be described by a third-order linear system

$$G(s) = \frac{X(s)}{W(s)} = \frac{K}{s^3 + a_0 s^2 + a_1 s + a_2} \tag{17}$$

with

$$\begin{cases} a_0 = \dfrac{1}{R_0 C_A} + \dfrac{b_s}{m} \\ a_1 = \dfrac{b_s}{m R_0 C_A} + \dfrac{k_s}{m} \\ a_2 = \dfrac{k_s}{m R_0 C_A} \\ K = \dfrac{k_{\rm amp} T_{\rm em}}{m R_0 C_A} \end{cases} \tag{18}$$

where $K, a_i, i = \{0, 1, 2\}$, are the parameters related to those parameters in (11) and (12). Thus, the general model of the piezoelectric positioning stage can be represented by a linear third-order plant (17) preceded by a hysteresis nonlinearity $P(v_{\rm in}(t))$. Fig. 3 shows the block diagram of the general model.

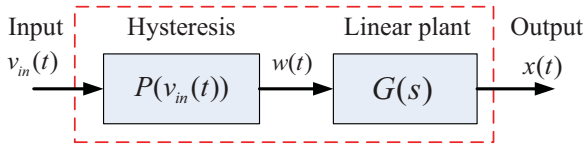

Fig. 3. Block diagram of the general model.

Remark: We should mention that there are two approaches to handle the hysteresis nonlinearity $H(q)$ in literature. One is by assuming $R_0 = 0$, the complete model is described by

$$m\ddot{x}(t) + b_s\dot{x}(t) + k_s x(t) = T_{\rm em}[k_{\rm amp} v_{\rm in}(t) - H(q)]. \tag{19}$$

Then, the Bouc–Wen model is utilized to describe the hysteresis term $H(q)$ [18], [19]. The second approach is to treat the term $v_{\rm in}(t) - \frac{H(f(v_{\rm in})}{k_{\rm amp}}$ as a new hysteresis nonlinearity [9]–[11]. For different approaches, the treatment for the controller designs is quite different because the hysteresis term in the first can be regarded as a sum component while the second is as a preceding component.

From (17) and (18), the parameters for the linear dynamic part cannot be obtained by simply using the specifications of the piezoelectric positioning stage, because the exact information on the parameters b_s, $T_{\rm em}$, and R_0 is generally not available. They are usually identified based on the applied input voltage and corresponding displacement.

In this study, the axiomatic-design-theory-based approach (ADTBA) [27] is utilized to identify parameters (K and a_i, $i =$ 0, 1, 2) of the linear plant (17) using experimental data of both frequency response and transient response. For model identification of the linear dynamic part, the third-order linear dynamic model is generally expressed as $k_p\omega_n^2/((\tau s + 1)(s^2 + 2\varsigma\omega_n s + \omega_n^2))$, where four parameters, i.e., k_p, ω, ς, and τ, should be determined. According to the ADTBA, the frequency response data are used to determine the parameters k_p and ω_n, and the transient response data are used to determine the parameters ς and τ. It is worthy of mentioning that small-amplitude input excitation signals should be applied to avoid distortion from the preceded hysteresis nonlinearity as much as possible [9], [28] and the higher sampling frequency (i.e., $f_s = 20$ kHz) is set to capture the fast dynamic response of the stage when the creep behavior can be conservatively neglected. The detailed steps are described as follows.

1) A small-amplitude band-limited white noise signal is used to excite the piezoelectric actuator. The system identification toolbox of MATLAB is adopted to obtain the frequency response of the stage as shown in Fig. 4 indicated by the solid blue line. The parameters k_p and ω_n can be directly obtained through the frequency response data.

2) A small-amplitude step signal is used to excite the piezoelectric actuator. Fig. 5(solid blue line) shows the transient response of the piezoelectric positioning stage that is captured during the first 6 ms. With the identified resonant frequency ω_n and the gain k_p in the first step, the transient response data are used to adjust time constant τ and damping coefficient ς.

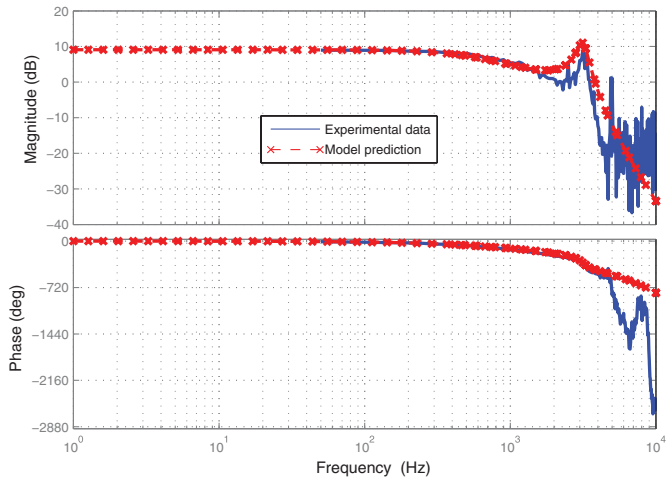

Fig. 4. Comparison of frequency response of the piezoelectric positioning stage (blue solid—experimental data; red dash—model simulation data).

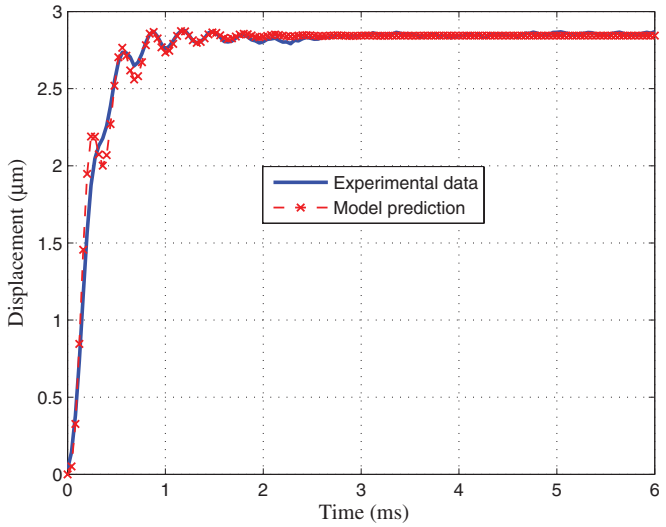

Fig. 5. Comparison of 1-V step response of the piezoelectric positioning stage in the first 6 ms (blue solid—experimental output response; red dash—model output response).

Based on the above two-step method, the identified parameters are compiled in Table II. Therefore, the linear dynamic plant $G(s)$ of the proposed model is expressed as

$$G(s) = \frac{4.767 \times 10^6}{s^3 + 7582s^2 + 4.1 \times 10^8 s + 1.677 \times 10^{12}}. \quad (20)$$

With the identified linear third-order model in (20), Figs. 4 and 5 show the comparisons of the frequency response and step response, respectively. It can be observed from Fig. 4 that the third-order model with the estimated parameters can reasonably capture the resonant dynamics in the frequency response. From Fig. 4, it should also be noted that both the magnitude and phase for the high frequency far beyond the natural frequency do not match the actual plant, which is also observed in other publications such as [9], [21], and [29]. The reasons could be a) the dynamic behavior of the mechanical part is modeled as a mass–spring–damper system in a frequency band within the natural frequency of vibration, which may not be appropriate for the high frequency far beyond the natural frequency; b) the lag of the measurement system is not taken into account; c) the piezoelectric positioning stage is described by a linear system preceded by a hysteresis term. However, Fig. 4 only shows the frequency response of the linear part, ignoring the hysteresis effect. Because a hysteresis term always causes the phase lag, depending on the hysteresis loops, this explains the obvious deviation in the phase plot at the high frequency shown in Fig. 4.

TABLE II
IDENTIFIED PARAMETERS OF THE GENERAL MODEL FOR THE PIEZOELECTRIC POSITIONING STAGE

Parameters	Value	Units
m	0.0515	kg
b_s	114	Ns/m
k_s	16.08	N/μm
R_0	40.5	Ω
C_A	4.6	μF
T_{em}	4.575	N/V
k_{amp}	10	-
a_0	7582	-
a_1	4.1×10^8	-
a_2	1.677×10^{12}	-
K	4.767×10^6	-

3) Description of the Hysteresis Nonlinearity: In the literature, many hysteresis models have been developed to describe the hysteresis nonlinearities such as physics-based models [30] and phenomenological hysteresis models [31]–[37]. In this paper, just for the model validation purpose, the backlash-like hysteresis model [38] is selected as an illustration. Certainly, other hysteresis models, for instance, the Preisach and Prandtl–Ishlinskii models, can also be selected. Without loss of generality, in what follows we use the backlash-like hysteresis model to validate the proposed model and develop a corresponding controller.

The dynamic backlash-like hysteresis model [38] is used to describe the term $w(t) = P(v_{\text{in}}(t))$ in (16), which is given as follows:

$$\frac{dw}{dt} = \alpha \left| \frac{dv_{\text{in}}}{dt} \right| (cv_{\text{in}} - w) + B_1 \frac{dv_{\text{in}}}{dt} \quad (21)$$

where α, c, and B_1 are constants, satisfying $c > B_1$. Since the hysteresis output $w(t)$ is always unknown (unmeasurable), the identification method should be adopted to obtain the parameters of the dynamic backlash-like hysteresis model (21) with the identified linear plant (20). In this study, the nonlinear least-squares fitting function is used and the parameters of the backlash-like hysteresis are obtained as $\alpha = 0.4195$, $c = 1.0341$, and $B_1 = 0.9592$.

4) Model Validation of the General Model: We are now ready to validate the proposed general model. Fig. 6 shows comparison of the experimental result and simulation result when a sinusoidal input signal $v_{\text{in}}(t) = 1 + 1\sin(2\pi 100t)$ (V) is used to drive the piezoelectric positioning stage. According to the comparison results, the proposed general model with the input

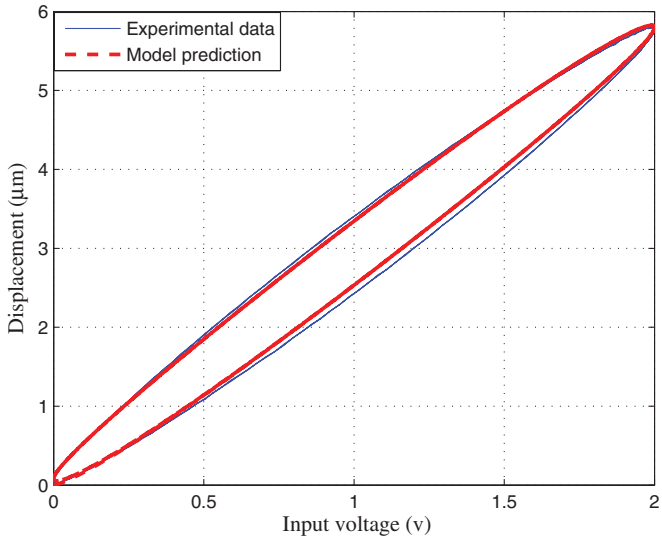

Fig. 6. Comparisons of the hysteresis loops between the experimental result and the simulation result at the frequency of 100 Hz (blue solid—experimental data; red dash—simulation data).

hysteresis nonlinearity can well describe the dynamics of the piezoelectric positioning stage and the hysteresis effect inherent to the PCA. It should be noted that the input hysteresis nonlinearities can also be described by other standard hysteresis models such as Preisach and Prandtl–Ishlinskii models. All the simulation results are similar, which illustrate the validity of the proposed general model.

IV. Robust Controller Design

With the proposed general model (16) and (17), the challenge turns to the controller design. However, as mentioned before, the identified parameters may not precisely describe the actual plant and the direct use of the identified parameters in the controller may lead to large control errors. To alleviate this difficulty, the robust control techniques shall be adopted in the paper because of using an inaccurate model.

The control objective in this paper is to design a robust control law for $v_{\rm in}(t)$ in (11) and (12) to force the plant states x to follow specified desired trajectories x_d, i.e., $x \to x_d$ within a desired accuracy as $t \to \infty$, where the desired trajectories x_d are continuous.

Since the dynamic model of the piezoelectric positioning stage is so similar to the traditional dc motor, except the hysteresis nonlinearity $H(q)$. Therefore, the challenge for control of the piezoelectric positioning stage system mainly lies on the way to handle the nonsmooth hysteresis nonlinearity $H(q)$. The common approach is to construct inverse hysteresis models to mitigate the hysteresis effect [37], and feedback control strategies are subsequently used to compensate for system dynamics [8], [39]–[42]. Due to the difficulty for the inverse construction, a direct robust approach was proposed in [38] and [43]. In this paper, following the same line as an illustration, a RAC is developed where the backlash-like dynamic model (21) is used to achieve the control objective. Certainly, other control methods can also be utilized as illustrations, depending on the choice of the hysteresis modeling approaches.

A. Backlash-Like Hysteresis Model

To describe the hysteresis nonlinearities $P(v_{\rm in}(t))$, the dynamic backlash-like hysteresis model has been introduced in (21). According to the analysis in [38], the differential (21) can be solved explicitly for v piecewise monotone

$$w(t) = P(v_{\rm in}(t)) = cv_{\rm in}(t) + d(v_{\rm in}) \tag{22}$$

with

$$d(v_{\rm in}) = [w_0 - cv_0]e^{-\alpha(v_{\rm in}-v_0)\mathrm{sgn}\dot{v}_{\rm in}} + e^{-\alpha v_{\rm in}(\mathrm{sgn}\dot{v}_{\rm in})}\int_{v_0}^{v_{\rm in}} [B_1 - c]e^{\alpha\zeta(\mathrm{sgn}\dot{v}_{\rm in})}d\zeta \tag{22b}$$

for $\dot{v}_{\rm in}$ constant and $w(t_0) = w_0$. For $d(v_{\rm in})$, it can be easily shown that if $w(v_{\rm in}; v_0, w_0)$ is the solution of (22) with initial values (v_o, w_0), then, if $\dot{v}_{\rm in} > 0\,(\dot{v}_{\rm in} < 0)$ and $v_{\rm in} \to +\infty\,(-\infty)$, one has

$$\lim_{v_{\rm in}\to+\infty} d(v_{\rm in}) = -\frac{c - B_1}{\alpha} \tag{23}$$

$$\left(\lim_{v_{\rm in}\to-\infty} d(v_{\rm in}) = \frac{c - B_1}{\alpha}\right). \tag{24}$$

From (23) and (24), we can see that the parameter α determines the rate at which $w(t)$ switches between $-((c - B_1)/\alpha)$ and $((c - B_1)/\alpha)$. The larger the parameter α is, the faster the transition in $w(t)$ is going to be.

B. Controller Design

In the aforementioned discussions, the piezoelectric positioning stage has been represented by a linear third-order plant (20) preceded by the input backlash-like hysteresis nonlinearity (22). To avoid heavy formulations in the controller designs, rather than designing a robust controller for the third-order dynamic system directly, a reduced order dynamic system is adopted as an illustration for the controller design. Such a treatment is also observed in [8] and [9]. To obtain a reduced-order model, it is worthy of mentioning that the maximum frequency of tracking trajectories addressed in the paper is around 100 Hz, which is generally true in industrial applications [28], [44]. From (20) and identified parameters, we can get that $\omega^3 < 7582\omega^2 \ll 4.1 \times 10^8\omega$ when $\omega \le 2\pi \times 100$. Therefore, the plant model can be approximately represented by a reduced first-order dynamic model

$$G_r(\mathrm{s}) = \frac{2.843 \times 10^{-6}}{0.0002445\mathrm{s} + 1}. \tag{25}$$

In order to verify the reduced dynamic system, Fig. 7 shows the comparison of the actual response and the reduced model simulation response, which clearly demonstrates that the reduced first-order model can well follow the actual response.

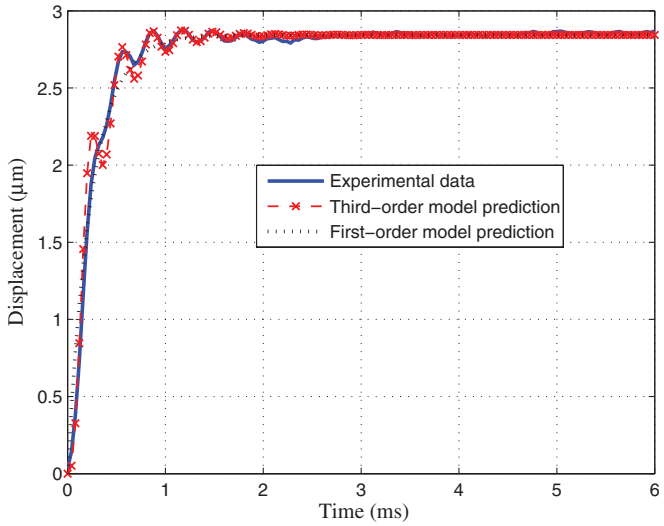

Fig. 7. Comparison of 1-V step response of the piezoelectric-actuated stage in the first 6 ms (blue solid—experimental output response; red dash—model output response; black dot—reduced-order model output response).

Based on the previous analysis, in the following development the controlled stage system will approximately be described as

$$\dot{x}(t) + ax(t) = bw(t) \tag{26}$$

$$w(t) = P(v_{\text{in}}(t)) \tag{27}$$

where a and b are unknown system parameters with uncertainties, $w(t)$ is the output of the hysteresis nonlinearity.

From the solution structure (22) of the hysteresis model (21) we see that the signal $w(t)$ is expressed as a linear function of the input signal $v_{\text{in}}(t)$ plus a bounded term. Substituting the solution expression (22) into the dynamic system (26), one can get

$$\dot{x}(t) + ax(t) = bcv_{\text{in}}(t) + bd(v_{\text{in}}). \tag{28}$$

For the development of a control law, the following standard assumptions about the system (28) are borrowed.

Assumption: The extents of the parameter uncertainties and uncertain nonlinearities satisfy

$$\theta \triangleq a/bc \in \Omega_\theta \triangleq \{\theta :\ \theta_{\min} \le \theta \le \theta_{\max}\} \tag{29}$$

$$\phi \triangleq 1/bc \in \Omega_\phi \triangleq \{\phi :\ \phi_{\min} \le \phi \le \phi_{\max}\} \tag{30}$$

$$d(v_{\text{in}}) \in \Omega_{dv_{\text{in}}} \triangleq \{d(v_{\text{in}}) :\ \|d(v_{\text{in}})\| \le \rho\} \tag{31}$$

where $\theta_{\min}$, $\theta_{\max}$, $\phi_{\min}$, and $\phi_{\max}$ are some known real numbers, ρ is a uniform bound constant.

In presenting the developed robust adaptive control law, the following definitions are required:

$$\widetilde{x} = x - x_d, \widetilde{\theta} = \widehat{\theta} - \theta, \widetilde{\phi} = \widehat{\phi} - \phi \tag{32}$$

where $\widetilde{x}$ represents the tracking error, $\widehat{\theta}$ is an estimate of θ, and $\widetilde{\phi}$ is an estimate of ϕ.

To achieve the required control objective, an integral filtered tracking error is defined as

$$s(t) = \left(\frac{d}{dt} + \lambda\right)\left(\int_0^t \widetilde{x}(\tau)d\tau\right), \quad \text{with } \lambda > 0 \tag{33}$$

where $s(t)$ can be rewritten as $s(t) = \widetilde{x}(t) + \lambda \int_0^t \widetilde{x}(\tau)d\tau$.

Rather than deriving the adaptive law with the filtered error $s(t)$, a tuning error is introduced

$$s_\epsilon = s - \epsilon \text{sat}(s/\epsilon) \tag{34}$$

where ϵ is an arbitrary positive constant and $\text{sat}(\cdot)$ is the standard saturation function defined as

$$\text{sat}(z) = \begin{cases} 1, & \text{for } z \ge 1 \\ z, & \text{for } -1 < z < 1 \\ -1, & \text{for } z \le -1. \end{cases} \tag{35}$$

For the piezoelectric-actuated nanopositioning system (28) subject to the notions discussed above, the following control and adaptation laws are proposed

$$v_{\text{in}}(t) = -k_d s + \widehat{\phi} u_{fd}(t) + \widehat{\theta} x(t) - k^* \text{sat}(s/\epsilon) \tag{36}$$

$$u_{fd}(t) = \dot{x}_d(t) - \lambda \widetilde{x}(t) \tag{37}$$

$$\dot{\widehat{\phi}} = \text{proj}(\widehat{\phi}, -\eta u_{fd} s_\epsilon) \tag{38}$$

$$\dot{\widehat{\theta}} = \text{proj}(\widehat{\theta}, -\gamma x s_\epsilon) \tag{39}$$

where $k_d > 0$, and k^* is control gain, satisfying $k^* \ge \rho/c_{\min}$, therein ρ is defined in (31). In addition, the parameters η and γ are positive constants determining the rates of adaptations, and $\text{proj}(\widehat{z},\ -y)$ is a projection operator, which is formulated as

$$\text{proj}(\widehat{z},\ -y) = \begin{cases} 0, & \text{if } \widehat{z} = z_{\max} \text{ and } y < 0 \\ -y, & \text{otherwise} \\ 0, & \text{if } \widehat{z} = z_{\min} \text{ and } y > 0. \end{cases} \tag{40}$$

According to the definition of the projection (40), the following properties [38] can be obtained:

(P1) $\widehat{\theta} \in \Omega_\theta$, if $\widehat{\theta}(t_0) \in \Omega_\theta$;

(P2) $\widehat{\phi} \in \Omega_\phi$, if $\widehat{\phi}(t_0) \in \Omega_\phi$;

(P3) $\|\text{proj}(z; -y)\| \le \|y\|$;

(P4) $-(z - z^*)^T \Lambda \text{proj}(z,\ -y) \ge -(z - z^*)^T \Lambda z$, where Λ is a positive definite symmetric matrix.

The stability of the closed-loop system described by (28), and (36)–(40) is established in the following theorem.

Theorem 1: For the plant in (28) with hysteresis nonlinearity (22) at the input subject to Assumption, the RAC specified by (36)–(40) ensures that if $\widehat{\theta}(t_0) \in \Omega_\theta$ and $\widehat{\phi}(t_0) \in \Omega_\phi$, all the closed-loop signals are bounded and the tracking error vector $\widetilde{x}(t)$ converges to $\Omega_\epsilon \triangleq \{\widetilde{x}(t) || \widetilde{x}| \le \epsilon\}$, such that $x \to x_d$ as $t \to \infty$.

Proof: See Appendix A. ■

Remarks:

1) It should be noted that the above controller development can only be thought of as an illustration. First of all, the analytical model (11) and (12) of the piezoelectric positioning stage may not necessarily be transferred into a linear system preceded by a hysteresis term. Second, even

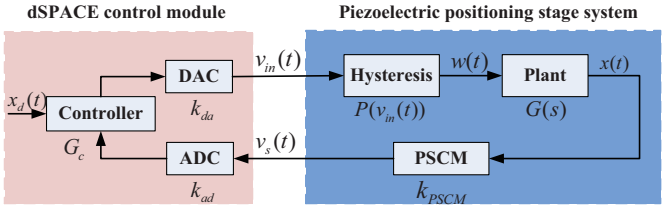

Fig. 8. Block diagram of the controlled system.

transferring the model of the stage into a linear system preceded by a hysteresis term, the controller can be designed without necessarily reducing to a low-order model. Third, it is still an open issue to select hysteresis models such as physics-based models [30] and phenomenological hysteresis models [31]–[37], which suit for the hysteresis description and controller designs. The proposed method can serve as initial step toward the development of a general control framework for the piezoelectric positioning stage.

2) The tuning error s_ϵ will disappear when the filtered error $|s| \leq \epsilon$, which shall be the equivalent of creating an adaptation dead band. It should be noticed that if ϵ is chosen too small, the linear region of the function sat(s/ϵ) will be too thin, which can result in the excitation of high-frequency fluctuations. As $\epsilon \to 0$, the function sat(s/ϵ) eventually becomes discontinuous. In such a case, the controller becomes a typical variable structure control scheme, which may cause chattering phenomena. This suggests that a tradeoff must be made between the value of ϵ and trajectory-following requirements.

V. Experimental Evaluation

In order to verify the proposed general model and the developed robust controller, an experimental platform is established based on the system description shown in Fig. 1, and several experiments are conducted with different motion trajectories. The dSPACE control board equipped with 16-bit analog-to-digital converters (ADCs) and 16-bit digital-to-analog converters (DACs) are adopted to implement the developed controller for high-performance motion tracking control in the MATLAB/Simulink environment. According to the specifications of the dSPACE-DS1104 control board, there is a fixed ratio of 10 for ADC and DAC channel in the dSPACE control module, that is, $k_{\rm da} = 10$, and $k_{\rm ad} = 1/10$. With the previous discussion, block diagram of the whole system is shown in Fig. 8.

The developed robust adaptive control algorithm is implemented into a S-function file in MATLAB using C language for the real-time control purpose at a sampling frequency of 10 kHz. According to the prior experimental tests, the bounds of the system parameters were estimated as $\theta \in [0.5,\ 4]$ and $\phi \in [0.0001,\ 0.005]$. Based on the priori experimental data, ρ and $c_{\min}$ were determined as $\rho = 0.18$ and $c_{\min} = 1$, which resulted in $k^* \geq 0.18$. In this study, k^* was selected as $k^* = 0.2$. In the adaption laws, the initial values for $\widehat{\theta}(0)$ and $\widehat{\phi}(0)$ were arbitrarily set to $\widehat{\theta}(0) = 1$ and $\widehat{\phi}(0) = 0.00075$. The adaptation rates

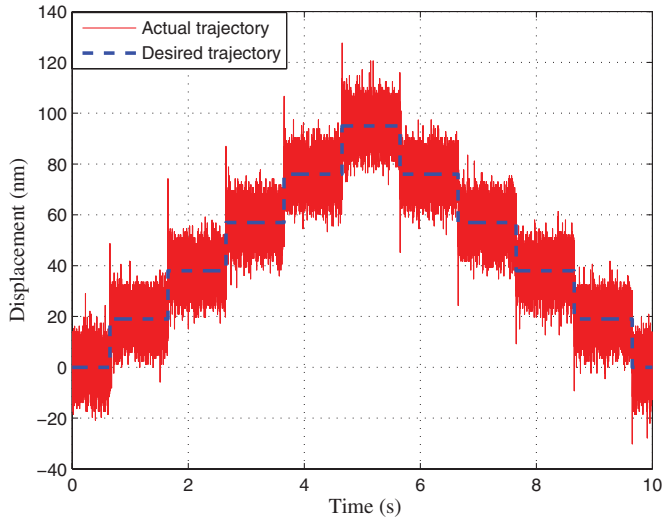

Fig. 9. Stepwise response.

were chosen as $\gamma = 3000$ and $\eta = 0.01$. The initial states were set to $x(0) = 3.8$ μm. The other parameters for the developed controller were $k_d = 1.5$, $\lambda = 1500$, and $\epsilon = 0.005$.

To quantify the performance of our controller, the following definitions will be used:

(D1) $e_m = \max(|x(t) - x_d(t)|)$: the maximum value of the error.

(D2) $e_{\rm rms} = \sqrt{(1/T)\int_0^T |x(t) - x_d(t)|^2 dt}$: the root mean square value of the error with T representing the total running time.

A. Point-to-Point Positioning

In the first experiment, we evaluate point-to-point positioning performance of the piezoelectric positioning stage using the developed RAC. Fig. 9 shows a stepwise response, where a fine positioning resolution of 19 nm is achieved. Besides, Fig. 10 shows the experimental results of 7.8-μm peak-to-peak square waves with 50% duty cycle and a period of 0.5 s. From Fig. 10(b), it can be seen that the piezoelectric positioning stage has a 6-ms rising time with a 1.5% overshoot and the response of the stage converges to the new set point after about 15 ms. The e_m and $e_{\rm rms}$ of steady-state error shown in Fig. 10(c) are about 20 and 4.58 nm, respectively. The point-to-point experimental results well demonstrate the high-speed and high-precision positioning response with the developed controller.

B. Sinusoidal Trajectory Tracking

To test the tracking ability of the developed controller, several sinusoidal trajectory motion tests are conducted to evaluate the tracking performance. Choosing the desired trajectory $x_d(t) = 3.8 + 3.8\sin(2\pi 100t)$ (μm), experimental results are shown in Fig. 11. Comparisons of the desired trajectories and the actual experimental results are shown in Fig. 11(a). Fig. 11(b) shows the tracking error with $e_m = 86.4$ nm and $e_m = 39.4$ nm, and the resulting input–output relation curves are shown in Fig. 11(c). We can see from Fig. 11 that hysteresis

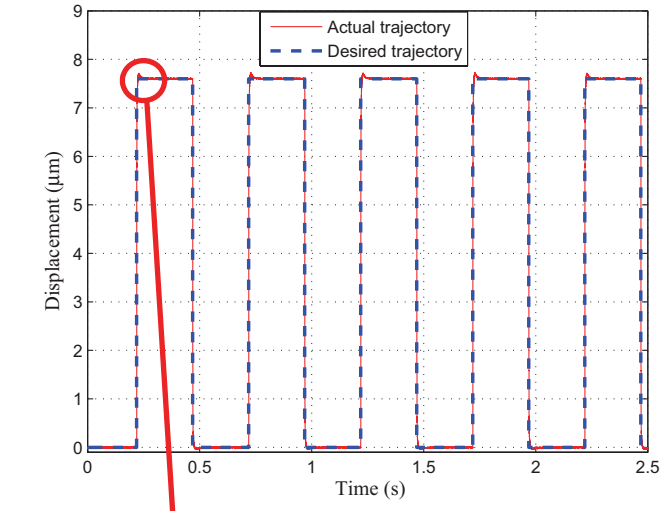

(a)

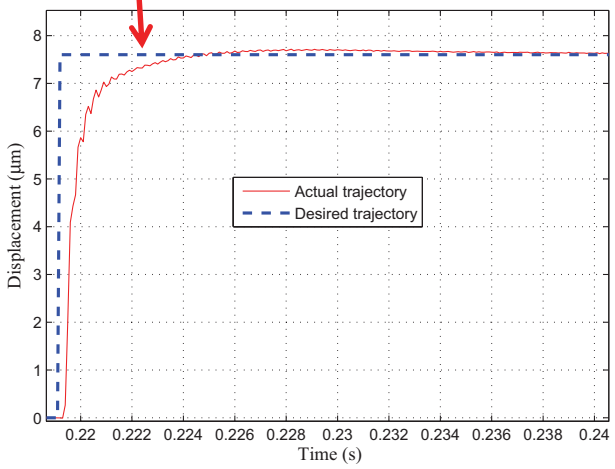

(b)

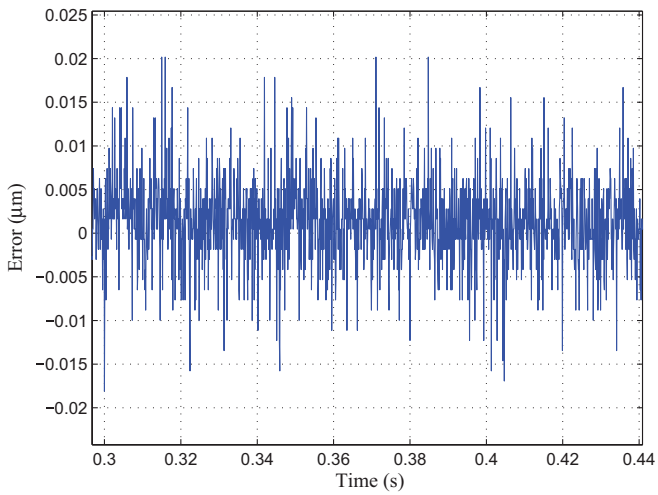

(c)

Fig. 10. Square-wave response. (a) Point-to-point positioning. (b) Zoom in of point-to-point positioning. (c) Steady-state error.

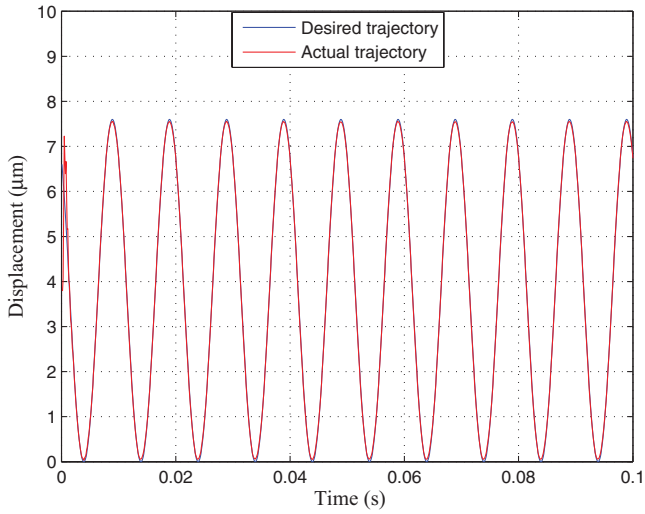

(a)

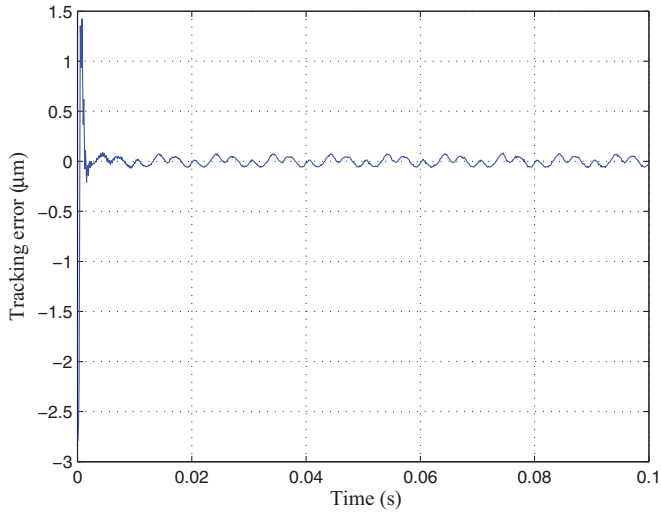

(b)

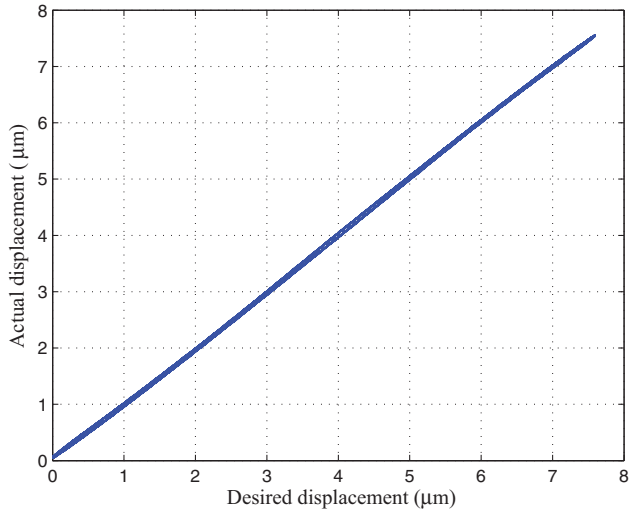

(c)

Fig. 11. Tracking control of sinusoidal trajectory at the frequency of 100 Hz. (a) Trajectory tracking (blue solid—desired trajectory, red solid—actual trajectory). (b) Tracking error. (c) Input–output relation curves.

TABLE III
TRACKING PERFORMANCE COMPARISONS OF RAC AND PIC WITH DIFFERENT FREQUENCIES (THE DESIRED TRAJECTORIES $x_d(t) = 3.8 + 3.8\sin(2\pi ft)$ (μm))

f (Hz)	Controller	e_m (μm)	e_{rms} (μm)
1	RAC	0.0273	0.0044
	PIC	0.0455	0.0138
10	RAC	0.0317	0.0056
	PIC	0.2056	0.1314
50	RAC	0.0484	0.0176
	PIC	0.8901	0.6144
100	RAC	0.0864	0.0394
	PIC	1.4401	1.0046

nonlinearity is well eliminated by the developed controller. In order to further clarify the performance of the developed controller, evaluations are made between the developed RAC and the traditional proportional integral controller (PIC), where the parameters of the PIC were selected as $k_p = 1.5$ and $k_i = 1500$ with the trial and error method. In this study, the PIC is adopted to show that the developed RAC improves tracking performance and robustness with the fixed designed parameters. As listed in Table III, it can be seen that comparison of tracking errors of the PIC and RAC is not obvious under lower input frequencies (around 10 Hz). However, with the increase of the frequency of the input trajectory, the tracking performance of the PIC is severely degraded. In contrast, the developed RAC presents a more robust performance with fixed designed parameters under different input frequencies. Particularly, compared with the PIC, the tracking errors e_m and $e_{\rm rms}$ of the RAC are reduced by 94% and 96%, respectively, at the input frequency of 100 Hz. It, therefore, demonstrates that the developed RAC is more suitable for control of the piezoactuated nanopositioning stage. In addition, it is worthy of mentioning that the tracking errors increase with the increase of the input frequencies.

C. Multifrequency Trajectory Tracking

Furthermore, motion tracking of multifrequency trajectories is undertaken to verify the robust control performance of the developed controller. The experimental results are shown in Fig. 12 with the frequencies of 10 and 100 Hz. Tracking of the desired trajectory, tracking error, and resulting input–output relation curves are shown in Fig. 12(a)–(c). From the plot of the actual position versus desired position as depicted in Fig. 12(c), the width of the hysteresis loops has been reduced to a lower level of 1.05% with comparison to 17.25% obtained by the open-loop test under the same input frequencies. From the experimental results depicted in Fig. 12, it is observed that the tracking errors caused by both the major-loop and minor-loop hysteresis nonlinearities are significantly suppressed.

Therefore, it can be concluded that the developed RAC under the proposed general model achieves excellent tracking performance and strong robustness at the presence of unknown hysteresis nonlinearity and parameter uncertainties, even in high-speed motion control applications.

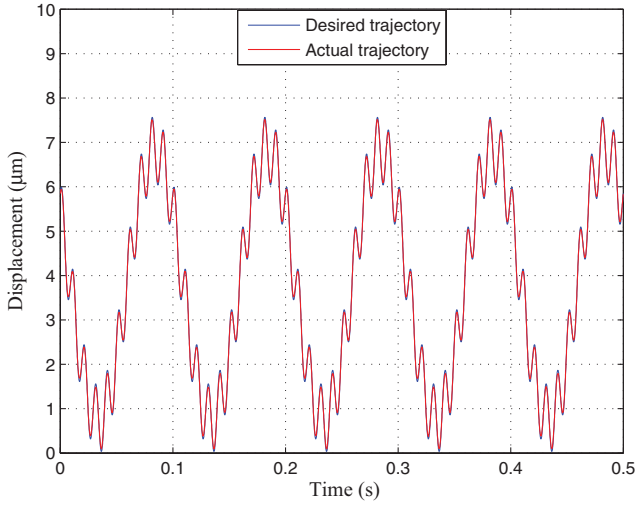

(a)

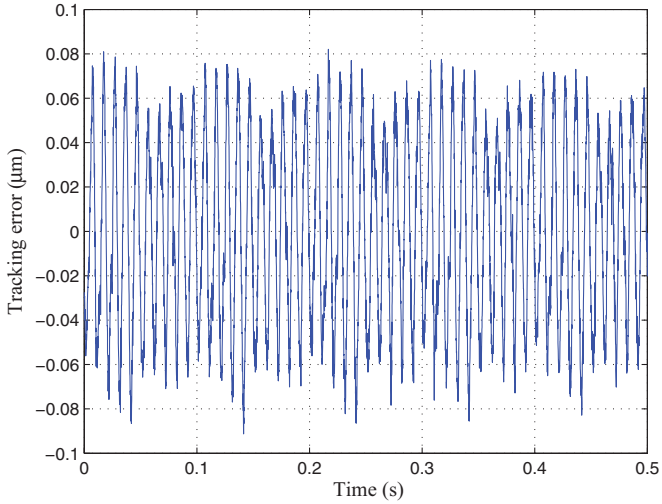

(b)

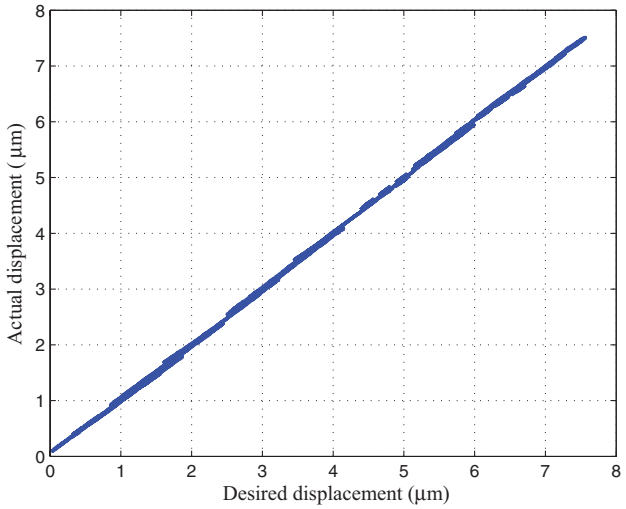

(c)

Fig. 12. Tracking control of multifrequency sinusoidal trajectories with the frequencies of 10 and 100 Hz. (a) Trajectory tracking (blue solid—desired trajectory, red solid—actual trajectory). (b) Tracking error. (c) Input–output relation curves.

VI. Conclusion

This paper presents a comprehensive study on modeling, controller design, and experimental evaluation for the motion control of piezoelectric positioning stages. Several distinct features of this paper are summarized as follows:

1) A general model of the piezoelectric positioning stage is first proposed to completely represent the dynamic behaviors of the stage including frequency response of the stage, voltage–charge hysteresis, and nonlinear electric behavior.

2) To illustrate the controller design with the proposed general model, a RAC is then developed for a reduced-order model of the stage with unknown parameters and hysteresis nonlinearity, where the hysteresis nonlinearity is described by a dynamic backlash-like model. The proposed control law ensures the boundedness of the closed-loop signals, and yields desired tracking precision.

3) Experimental tests on a prototype platform with different motion trajectories are conducted to verify the developed robust control law. Experimental results demonstrate the excellent tracking performance, which validates the feasibility and effectiveness of the proposed approach.

It should be noted that the proposed method can be thought of as an initial step toward the development of a general control framework for the piezoelectric positioning stage. As a matter of fact, the proposed general model provides a base for various controller designs, depending on applications.

Appendix

Proof of Theorem 1

Proof: To establish global boundedness, define a Lyapunov function candidate as

$$V(t) = \frac{1}{2}\left[\frac{1}{bc}{s_\epsilon}^2 + \frac{1}{\gamma}\widetilde{\theta}^T\widetilde{\theta} + \frac{1}{\eta}\widetilde{\phi}^2\right]. \tag{41}$$

The first derivative of the above equation is

$$\dot{V} = \frac{1}{bc}s_\epsilon\dot{s_\epsilon} + \frac{1}{\gamma}\widetilde{\theta}^T\dot{\widehat{\theta}} + \frac{1}{\eta}\widetilde{\phi}\dot{\widehat{\phi}}. \tag{42}$$

Using (26) the time derivative of the sliding surface (33) can be written as

$$\dot{s} = -ax(t) - \dot{x}_d(t) + \lambda\widetilde{x}(t) + bcv_{\text{in}}(t) + bd(t). \tag{43}$$

Applying the control laws (36)–(39), the above (43) can be rewritten as

$$\dot{s}(t) = -u_{fd}(t) - ax(t) + bc[-k_d s + \widehat{\phi}u_{fd}(t) + \widehat{\theta}x(t) - k^*\text{sat}(s/\epsilon)] + bd(t). \tag{44}$$

In the following proof, there are only two cases to be examined.

Case 1 ($|s| \le \epsilon$): Since the discontinuity at $|s| = \epsilon$ is of the first kind and $s_\epsilon = 0$ when $|s| \le \epsilon$, it follows that the derivative $\dot{V}$ exists for all s, and is given by

$$\dot{V}(t) = 0, \quad \text{when } |s| \le \epsilon. \tag{45}$$

Case 2 ($|s| > \epsilon$): Noting the fact $s_\epsilon\dot{s_\epsilon} = s_\epsilon\dot{s}$ and using (44), (42) becomes

$$\dot{V} = -k_d s s_\epsilon + s_\epsilon\left[-k^* sat(s/\epsilon) + \widetilde{\phi}u_{fd}(t) + \widetilde{\theta}x(t) + \frac{d(t)}{c}\right] + \frac{1}{\gamma}\widetilde{\theta}^T\dot{\widehat{\theta}} + \frac{1}{\eta}\widetilde{\phi}\dot{\widehat{\phi}}. \tag{46}$$

The above equation can be simplified, by the choice of s_ϵ, as

$$\dot{V} \le -k_d {s_\epsilon}^2 + s_\epsilon\left[-k^*\text{sat}(s/\epsilon) + \widetilde{\phi}u_{fd}(t) + \widetilde{\theta}x(t) + \frac{d(t)}{c}\right] + \frac{1}{\gamma}\widetilde{\theta}^T\dot{\widehat{\theta}} + \frac{1}{\eta}\widetilde{\phi}\dot{\widehat{\phi}}. \tag{47}$$

Utilizing the adaptive laws given in (38)–(39) and the properties of the projection operators

$$\widetilde{\theta}\text{proj}(\widehat{\theta},\ -\gamma s_\epsilon) \le -\gamma x(t)\widetilde{\theta}s_\epsilon,$$
$$\widetilde{\phi}\text{proj}(\widehat{\phi},\ -\eta u_{fd}s_\epsilon) \le -\eta\widetilde{\phi}u_{fd}s_\epsilon.$$

We have

$$\begin{aligned}\dot{V} &\le -k_d s_\epsilon^2 - k^* s_\epsilon \text{sat}(\frac{s}{\epsilon}) + s_\epsilon\frac{d(t)}{c}\\ &\le -k_d s_\epsilon^2 - k^*|s_\epsilon| + \frac{\rho}{c_{\min}}|s_\epsilon|\\ &\le -k_d s_\epsilon^2.\end{aligned} \tag{48}$$

In the above, the relationship, $|s_\epsilon| = s_\epsilon\text{sat}(s/\epsilon)$ for $|s_\epsilon| > \epsilon$ and $k^* \ge \frac{\rho}{c_{\min}}$ has been used.

From (45) and (48), one can get that V is a Lyapunov function, which leads to global boundedness of s_ϵ, $\widetilde{\theta}$, and $\widetilde{\phi}$. From the definition of s_ϵ, $s(t)$ is also bounded. It can be shown that if $\widetilde{x}(0)$ is bounded, then $\widetilde{x}(t)$ is also bounded for all t. Since $x_d(t)$ is bounded by design, $x(t)$ must also be bounded. To complete the proof and establish asymptotic convergence of the tracking error, it is necessary to show that $s_\epsilon \to 0$ as $t \to \infty$. This is accomplished by applying Barbalat's lemma [38], [45] to the continuous, nonnegative function

$$V_1(t) = V(t) - \int_0^t (\dot{V}(\tau) + k_d s_\epsilon^2(\tau))d\tau \tag{49}$$

with

$$\dot{V}_1 = -k_d s_\epsilon^2(t). \tag{50}$$

It can easily be shown that every term in (44) is bounded, hence $\dot{s}$, and $\dot{s_\epsilon}$ are bounded. Thus, it can be demonstrated that $\dot{V}_1$ is a uniformly continuous function of time. Since V_1 is bounded below by 0, and $\dot{V}_1 \le 0$ for all t, use of Barbalat's lemma proves that $\dot{V}_1 \to 0$. From (49), it can be demonstrated that $s_\epsilon \to 0$ as $t \to \infty$. According to the results in [38] and [45], the tracking error vector $\widetilde{x}(t)$ converges to $\Omega_\epsilon \triangleq \{\widetilde{x}(t)||\widetilde{x}| \le \epsilon\}$, such that $x \to x_d$ as $t \to \infty$. ■

References

[1] S. Devasia, E. Eleftheriou, and S. O. R. Moheimani, "A survey of control issues in nanopositioning," *IEEE Trans. Control Syst. Technol.*, vol. 15, no. 5, pp. 802–823, Sep. 2007.

[2] M. Grossard, M. Boukallel, N. Chaillet, and C. Rotinat-Libersa, "Modeling and robust control strategy for a control-optimized piezoelectric microgripper," *IEEE/ASME Trans. Mechatronics*, vol. 16, no. 4, pp. 674–683, Aug. 2011.
[3] R. Merry, M. Maassen, M. Molengraft, N. Wouw, and M. Steinbuch, "Modeling and waveform optimization of a nano-motion piezo stage," *IEEE/ASME Trans. Mechatronics*, vol. 16, no. 4, pp. 615–626, Aug. 2011.
[4] S. M. Salapaka and M. V. Salapaka, "Scanning probe microscopy," *IEEE Control Syst. Mag.*, vol. 28, no. 2, pp. 65–83, 2008.
[5] B. J. Kenton and K. K. Leang, "Design and control of a three-axis serial-kinematic high-bandwidth nanopositioner," *IEEE/ASME Trans. Mechatronics*, vol. 17, no. 2, pp. 356–369, Apr. 2012.
[6] S. Salapaka, A. Sebastian, J. P. Cleveland, and M. V. Salapaka, "High bandwidth nano-positioner: A robust control approach," *Rev. Sci. Instrum.*, vol. 793, no. 9, pp. 3232–3241, 2002.
[7] H. C. Liaw, B. Shirinzadeh, and J. Smith, "Enhanced sliding mode motion tracking control of piezoelectric actuators," *Sens. Actuators A, Phys.*, vol. 138, no. 1, pp. 194–202, 2007.
[8] J. Shen, W. Jywe, H. Chiang, and Y. Shu, "Precision tracking control of a piezoelectric-actuated system," *Presicion Eng.*, vol. 32, no. 2, pp. 71–78, 2008.
[9] J. H. Zhong and B. Yao, "Adaptive robust precision motion control of a piezoelectric positioning stage," *IEEE Trans. Control Syst. Technol.*, vol. 16, no. 5, pp. 1039–1046, Sep. 2008.
[10] X. K. Chen and T. Hisayam, "Adaptive sliding-mode position control for piezo-actuated stage," *IEEE Trans. Ind. Electron.*, vol. 55, no. 11, pp. 3927–3934, Nov. 2008.
[11] S. Bashash and N. Jalili, "Robust adaptive control of coupled parallel piezo-flexural nanopositioning stages," *IEEE/ASME Trans. Mechatronics*, vol. 14, no. 1, pp. 11–20, Feb. 2009.
[12] U. X. Tan, W. T. Latt, C. Y. Shee, and W. T. Ang, "A low-cost flexure-based handheld mechanism for micromanipulation," *IEEE/ASME Trans. Mechatronics*, vol. 16, no. 4, pp. 773–778, Aug. 2011.
[13] L. J. Lai, G. Y. Gu, and L. M. Zhu, "Design and control of a decoupled two degree of freedom translational parallel micro-positioning stage," *Rev. Sci. Instrum.*, vol. 83, no. 4, pp. 045105-1–045105-17, 2012.
[14] S. Polit and J. Dong, "Development of a high-bandwidth XY nanopositioning stage for high-rate micro-/nanomanufacturing," *IEEE/ASME Trans. Mechatronics*, vol. 16, no. 4, pp. 724–733, Aug. 2011.
[15] M. Goldfarb and N. Celanovic, "Modeling piezoelectric stack actuators for control of micromanipulation," *IEEE Control Syst. Mag.*, vol. 17, no. 3, pp. 69–79, Jun. 1997.
[16] H. J. M. T. A. Adriaens, W. L. D. Koning, and R. Banning, "Modeling piezoelectric actuators," *IEEE/ASME Trans. Mechatronics*, vol. 5, no. 4, pp. 331–341, Dec. 2000.
[17] Y. S. Gao, D. W. Zhang, and C. W. Yu, "Dynamic modeling of a novel workpiece table for active surface grinding control," *Int. J. Mach. Tools Manuf.*, vol. 41, no. 4, pp. 609–624, 2001.
[18] C. J. Lin and S. Y. Chen, "Evolutionary algorithm based feedforward control for contouring of a biaxial piezo-actuated stage," *Mechatronics*, vol. 19, no. 6, pp. 829–839, 2009.
[19] Y. Li and Q. Xu, "Adaptive sliding mode control with perturbation estimation and PID sliding surface for motion tracking of a piezo-driven micromanipulator," *IEEE Trans. Control Syst. Technol.*, vol. 18, no. 4, pp. 798–810, Jul. 2010.
[20] H. M. S. Georgiou and R. B. Mrad, "Electromechanical modeling of piezoceramic actuators for dynamic loading applications," *J. Dyn. Syst., Meas., Control*, vol. 128, no. 5, pp. 558–567, 2006.
[21] M. Quant, H. Elizalde, A. Flores, R. Ramirez, P. Orta, and G. Song, "A comprehensive model for piezoceramic actuators: modelling, validation and application," *Smart Mater. Struct.*, vol. 18, no. 12, 2009.
[22] G. Tao and F. L. Lewis, *Adaptive Control of Nonsmooth Dynamic Systems*. New York: Springer-Verlag, 2001.
[23] M. Salah, M. McIntyre, D. Dawson, and J. Wagner, "Robust tracking control for a piezoelectric actuator," in *Proc. Amer. Control Conf.*, Jul. 2007, pp. 106–111.
[24] P. Ronkanen, P. Kallio, M. Vilkko, and H. N. Koivo, "Displacement control of piezoelectric actuators using current and voltage," *IEEE/ASME Trans. Mechatronics*, vol. 16, no. 1, pp. 160–166, Feb. 2011.
[25] F. Giri, Y. Rochdi, F. Z. Chaoui, and A. Brouri, "Identification of Hammerstein systems in presence of hysteresis-backlash and hysteresis-relay nonlinearities," *Automatica*, vol. 44, no. 3, pp. 767–775, 2008.
[26] Q. Xu and Y. Li, "Dahl model-based hysteresis compensation and precise positioning control of an XY parallel micromanipulator with piezoelectric actuation," *J. Dyn. Syst., Meas., Control*, vol. 132, no. 4, p. 041011, 2010.
[27] J. W. Li, X. B. Chen, and W. J. Zhang, "Axiomatic-design-theory-based approach to modeling linear high order system dynamics," *IEEE/ASME Trans. Mechatronics*, vol. 16, no. 2, pp. 341–350, Apr. 2011.
[28] K. K. Leang and S. Devasia, "Feedback-linearized inverse feedforward for creep, hysteresis, and vibration compensation in AFM piezoactuators," *IEEE Trans. Control Syst. Technol.*, vol. 15, no. 5, pp. 927–935, Sep. 2007.
[29] M. Rakotondrabe, Y. Haddab, and P. Lutz, "Quadrilateral modelling and robust control of a nonlinear piezoelectric cantilever," *IEEE Trans. Control Syst. Technol.*, vol. 17, no. 3, pp. 528–539, May 2009.
[30] D. C. Jiles and D. L. Atherton, "Theory of ferromagnetic hysteresis," *J. Magn. Magn. Mater.*, vol. 61, nos. 1–2, pp. 48–60, 1986.
[31] M. Krasnosel'skii and P. Pokrovskii, *Systems with Hysteresis*. New York: Springer, 1989.
[32] P. Ge and M. Jouaneh, "Generalized Preisach model for hysteresis nonlinearity of piezoceramic actuators," *Precision Eng.*, vol. 20, no. 2, pp. 99–111, 1997.
[33] K. Kuhnen, "Modeling, identification and compensation of complex hysteretic nonlinearities: A modified Prandtl-Ishlinskii approach," *Eur. J. Control*, vol. 9, no. 4, pp. 407–418, 2003.
[34] M. A. Janaideh, S. Rakheja, and C. Y. Su, "An analytical generalized Prandtl-Ishlinskii model inversion for hysteresis compensation in micropositioning control," *IEEE/ASME Trans. Mechatronics*, vol. 16, no. 4, pp. 734–744, Aug. 2011.
[35] G. Y. Gu and L. M. Zhu, "Modeling of rate-dependent hysteresis in piezoelectric actuators using a family of ellipses," *Sens. Actuators A, Phys.*, vol. 165, no. 2, pp. 202–209, 2011.
[36] C. Visone, "Hysteresis modelling and compensation for smart sensors and actuators," *J. Phys., Conf. Series*, vol. 138, no. 1, p. 012028, 2008.
[37] P. Krejci and K. Kuhnen, "Inverse control of systems with hysteresis and creep," *Proc. Inst. Elect. Eng.—Control Theory Appl.*, vol. 148, no. 3, pp. 185–192, 2001.
[38] C. Y. Su, Y. Stepanenko, J. Svoboda, and T. P. Leung, "Robust adaptive control of a class of nonlinear systems with unknown backlash-like hysteresis," *IEEE Trans. Autom. Control*, vol. 45, no. 12, pp. 2427–2432, Dec. 2000.
[39] P. Ge and M. Jouaneh, "Tracking control of a piezoceramic actuator," *IEEE Trans. Control Syst. Technol.*, vol. 4, no. 3, pp. 209–216, May 1996.
[40] G. Song, J. Q. Zhao, X. Q. Zhou, and J. A. D. Abreu-Garcia, "Tracking control of a piezoceramic actuator with hysteresis compensation using inverse Preisach model," *IEEE/ASME Trans. Mechatronics*, vol. 10, no. 2, pp. 198–209, Apr. 2005.
[41] U. X. Tan, W. T. Latt, F. Widjaja, C. Y. Shee, C. N. Riviere, and W. T. Ang, "Tracking control of hysteretic piezoelectric actuator using adaptive rate-dependent controller," *Sens. Actuators A, Phys.*, vol. 150, no. 1, pp. 116–123, 2009.
[42] G. Y. Gu and L. M. Zhu, "High-speed tracking control of piezoelectric actuators using an ellipse-based hysteresis model," *Rev. Sci. Instrum.*, vol. 81, no. 8, pp. 085104-1–085104-9, 2010.
[43] Q. Q. Wang and C. Y. Su, "Robust adaptive control of a class of nonlinear systems including actuator hysteresis with Prandtl-Ishlinskii presentations," *Automatica*, vol. 42, no. 5, pp. 859–867, 2006.
[44] S. S. Aphale, S. Devasia, and S. O. R. Moheimani, "High-bandwidth control of a piezoelectric nanopositioning stage in the presence of plant uncertainties," *Nanotechnology*, vol. 19, no. 12, p. 125503, 2008.
[45] E. J. J. Slotine and W. P. Li, *Applied Nonlinear Control*. Englewood Cliffs, NJ: Prentice-Hall, 1991.

Guo-Ying Gu (S'10) received the B.E. degree (Hons) in electronic engineering from Shanghai Jiao Tong University, Shanghai, China, in 2006, where he is currently working toward the Ph.D. degree in mechanical engineering.

He was a Visiting Researcher at Concordia University, Montreal, QC, Canada, from October 2010 to March 2011 and November 2011 to March 2012. His research interests include motion control of precision mechatronic systems, robust control, and modeling and control of smart material actuators with hysteresis.

Mr. Gu received the Scholarship Award for Excellent Doctoral Student granted by the Ministry of Education of China in 2011 and the Best Conference Paper Award at the 2011 IEEE International Conference on Information and Automation.

Li-Min Zhu (M'12) received the B.E. (Hons) and Ph.D. degrees in mechanical engineering from Southeast University, Nanjing, China, in 1994 and 1999, respectively.

From November 1999 to January 2002, he was a Postdoctoral Research Fellow at Huazhong University of Science and Technology, Wuhan, China. In March 2002, he was appointed as an Associate Professor at the Robotics Institute, Shanghai Jiao Tong University, Shanghai, China, where he has been a Professor since August 2005 in the School of Mechanical Engineering and is currently with the State Key Laboratory of Mechanical System and Vibration. He was a Visiting Scholar at Monash University, Clayton, Australia (from September 1997 to May 1998), and the City University of Hong Kong, Kowloon, Hong Kong (from December 2000 to March 2001). His research interests include mechatronics, computer-aided design/computer-aided manufacturing, and mechanical signature analysis.

Chun-Yi Su (SM'98) received the Ph.D. degree from South China University of Technology, Guangzhou, China, in 1990.

He is currently with the College of Automation Science and Engineering, South China University of Technology, Guangzhou, China, on leave from Concordia University, Montreal, QC, Canada. Prior to joining Concordia University in 1998, he was at the University of Victoria from 1991 to 1998. He conducts research on the application of automatic control theory to mechanical systems. He is particularly interested in control of systems involving hysteresis nonlinearities. He is the author or coauthor of more than 300 publications, which have appeared in journals, as book chapters, and in conference proceedings.

Dr. Su has served as an Associate Editor of the IEEE TRANSACTIONS ON AUTOMATIC CONTROL and the IEEE TRANSACTIONS ON CONTROL SYSTEMS TECHNOLOGY, and the *Journal of Control Theory and Applications*. He is on the Editorial Board of 14 journals, including the IFAC journals *Control Engineering Practice* and *Mechatronics*. He has also severed many conferences as an organizing committee member, including as General Co-Chair of the 2012 IEEE International Conference on Mechatronics and Automation and as Program Chair of the 2007 IEEE Conference on Control Applications.

Han Ding (M'97–SM'00) received the Ph.D. degree from Huazhong University of Science and Technology (HUST), Wuhan, China, in 1989.

Supported by the Alexander von Humboldt Foundation, he was at the University of Stuttgart, Stuttgart, Germany, from 1993 to 1994. He was at the School of Electrical and Electronic Engineering, Nanyang Technological University, Singapore, from 1994 to 1996. He has been a Professor at HUST since 1997. He is also the Director of the State Key Laboratory of Digital Manufacturing Equipment and Technology, HUST. He is a "Cheung Kong" Chair Professor at Shanghai Jiao Tong University, Shanghai, China. His research interests include robotics, multiaxis machining, and equipment automation

Dr. Ding is a Technical Editor of the IEEE/ASME TRANSACTIONS ON MECHATRONICS. He serves as a Guest Editor and a Technical Committee Member for semiconductor manufacturing automation of the IEEE Robotics and Automation Society. He has organized and chaired many technical sessions and workshops of various international conferences.